Observation of highly efficient second-harmonic generation at the nanoscale driven by bound states in the continuum

Koshelev, Kirill, Kruk, Sergey, Melik-Gaykazyan, Elizaveta, Choi, Jae-Hyuck, Bogdanov, Andrey, et al.

Kirill Koshelev, Sergey Kruk, Elizaveta Melik-Gaykazyan, Jae-Hyuck Choi, Andrey Bogdanov, Hong-Gyu Park, Yuri Kivshar, "Observation of highly efficient second-harmonic generation at the nanoscale driven by bound states in the continuum," Proc. SPIE 11290, High Contrast Metastructures IX, 112900C (26 February 2020); doi: 10.1117/12.2544231

SPIE.

Event: SPIE OPTO, 2020, San Francisco, California, United States

Observation of highly efficient second-harmonic generation at the nanoscale driven by bound states in the continuum

Kirill Koshelev[a,b], Sergey Kruk[a], Elizaveta Melik-Gaykazyan[a,c], Jae-Hyuck Choi[d], Andrey Bogdanov[b], Hong-Gyu Park[d], and Yuri Kivshar[a,b]

[a]Nonlinear Physics Center, Australian National University, Canberra ACT 2601, Australia
[b]Department of Physics and Engineering, ITMO University, St. Petersburg 197101, Russia
[c]Faculty of Physics, Lomonosov Moscow State University, Moscow 119991, Russia
[d]Department of Physics, Korea University, Seoul 02841, Republic of Korea

ABSTRACT

Recent developments in the physics of Mie-resonant high-index dielectric nanostructures suggested a promising pathway to improve efficiencies of the nonlinear light conversion beyond the limits imposed by plasmonics. Here, we employ the concept of bound states in the continuum to experimentally demonstrate a sharp enhancement of the second-harmonic generation efficiency at localized states formed via destructive interference of two leaky modes. For an AlGaAs subwavelength disk with optimized parameters, pumped with a structured light and placed on an engineered multilayered substrate, we observe the record-high conversion efficiency compared to the previous demonstrations with isolated subwavelength resonators.

Keywords: Second-harmonic generation, bound states in the continuum, meta-optics, subwavelength resonator, nanoantenna, structured light

1. INTRODUCTION

The study of resonant dielectric nanostructures with large refractive index is a new research direction in nanoscale optics and metamaterial-inspired nanophotonics.[1,2] Many concepts of all-dielectric resonant nanophotonics are driven by the idea to employ subwavelength dielectric nanoparticles with Mie resonances as "meta-atoms" for creating highly efficient optical metasurfaces and metadevices.[3,4] Precise engineering of optical resonances results in many fascinating phenomena such as perfect reflection, broadband transmission, complete control of phase and polarization, imaging with subwavelength resolution. The pronounced resonant properties of high-index dielectric nanoparticles along with low-cost fabrication and compatibility with planar technology make high-index nanoscale structures prospective candidates to complement or even replace different plasmonic components in a range of potential applications.[5] Moreover, many concepts which had been developed for plasmonic structures but could not be fully employed due to strong losses of metals, can now be realized based on low-loss dielectric structures.

High-index dielectric meta-atoms can support both electric and magnetic Mie resonances in the visible and mid-IR spectral ranges, which can be tailored by the nanoparticle geometry. To emphasize the importance of optically-induced magnetic response, the field of all-dielectric resonant nanophotonics is often termed as meta-optics. The study of Mie-resonant silicon nanoparticles have recently received considerable attention for applications in nanophotonics and metamaterials[6] including optical nanoantennas, wavefront-shaping metasurfaces, and nonlinear frequency generation.

The physics and applications of all-dielectric resonant nanophotonics could be extended substantially by employing the concept of bound states in the continuum (BICs), which present localized states with energies embedded in the continuous spectrum of radiating waves. BICs were predicted as a mathematical curiosity in quantum mechanics long time ago.[7] In spite of the fact that the system proposed in that work has never been implemented experimentally, for last years, the beautiful physics of BIC is attracting very broad attention in

Further author information: (Send correspondence to K.K.)
K.K.: E-mail: kirill.koshelev@anu.edu.au, Telephone: +61 410 269 103

High Contrast Metastructures IX, edited by Connie J. Chang-Hasnain, Andrei Faraon, Weimin Zhou, Proc. of SPIE Vol. 11290, 112900C · © 2020 SPIE · CCC code: 0277-786X/20/$21 · doi: 10.1117/12.2544231

photonics,[8–12] primarily because they provide a simple way to achieve very large quality factors (Q factors) for photonic crystals,[13,14] metasurfaces,[15] and even subwavelength isolated resonators.[16]

The key idea underlying the physics of bound states in the continuum is vanishing coupling between the resonant mode and all radiation channels of a surrounding space. In practice, infinitely high Q factors of BICs are limited by a finite size of samples, material absorption, structural disorder and surface scattering.[17] As a result, BICs are transformed into resonant states with a giant Q factor often treated as quasi-BICs. Remarkably, quasi-BICs can be formed even in a single subwavelength high-index dielectric resonator by tuning the structure parameters into the so-called supercavity regime.[18,19]

Here, we discuss the recent advances in the physics of bound states in the continuum in application to isolated subwavelength particles. We pay special attention to novel opportunities for nonlinear nanophotonics due to the fact that high-Q states (quasi-BICs) supported by subwavelength particles are associated with large energy concentration inside the particle volume. We observe experimentally a BIC-associated optical mode for a nanoparticle of the specific parameters providing the high value of second-harmonic generation efficiency.

2. MODE ANALYSIS FOR INDIVIDUAL SUBWAVELENGTH DISKS

In this section, we explain the mechanism of formation of quasi-BICs in an individual cylindrical nanoresonator. For numerical calculations we consider individual AlGaAs (20% Al) nanodisks placed on a substrate made of a commercial film of 300-nm ITO on glass with an added 350-nm thick SiO2 spacer.

The eigenmodes of a disk resonator in the free space can be rigorously classified according to their azimuthal order ($m = 0, \pm1, \pm2, \ldots$) with respect to the disk axis and their parity with respect to the up-down inversion along the disk axis ($p = 0, 1$). Away from the avoided resonance crossings (ARCs) of the frequency curves, each mode of the cylindrical nanoresonator can be also sorted in one of two groups distinguished by the number of oscillations in the radial and axial directions. This sorting is not rigorous, but it is qualitatively justified and is useful to categorize the modes. The justification can be done by considering the extreme case of an infinitely long cylinder, where radial modes represent the well-known Mie modes while axial modes appear only for a finite length of the cylinder.

We select a pair of modes from different groups (one radial and one axial) with the same m and p. With the change of the cylinder aspect ratio their frequencies change differently because of their distinct nature. In the vicinity of the specific aspect ratios, the mode dispersion curves tend to cross. However, the nanoresonator has open boundaries which make it a non-Hermitian electromagnetic system and allow the so-called internal and external coupling between its modes. In the strong coupling regime, the mode dispersion curves exhibit the ARC behavior and the mode radiative losses change due to the external coupling. Near the ARC the modes are hybrid with a combination of radial or axial oscillations and thus do not belong to any of the defined groups. Here, we also note that modes with different m or p do not interact and their frequency curves always cross.

The proper quantitative description of the mode hybridization can be achieved by analyzing the eigenfunction evolution in the vicinity of the ARC of two modes [see Fig. 1A]. We denote the hybrid eigenfunctions of the cylinder resonator as $\varphi_{1,2}$, they are given by the linear combination of the eigenfunctions of the uncoupled radial and axial modes $\varphi_{a,b}$, respectively

$$\varphi_{1,2} = C^a_{1,2}\varphi_a + C^b_{1,2}\varphi_b. \tag{1}$$

The complex coefficients $C^{a,b}_{1,2}$ can be determined by solving the 2x2 matrix equation (*22*)

$$\begin{bmatrix} \omega_\mathrm{a} - i\gamma_\mathrm{a} & 0 \\ 0 & \omega_\mathrm{b} - i\gamma_\mathrm{b} \end{bmatrix} \begin{bmatrix} C^a_{1,2} \\ C^b_{1,2} \end{bmatrix} = \omega_{1,2} \begin{bmatrix} 1+V_\mathrm{aa} & V_\mathrm{ab} \\ V_\mathrm{ba} & 1+V_\mathrm{bb} \end{bmatrix} \begin{bmatrix} C^a_{1,2} \\ C^b_{1,2} \end{bmatrix}. \tag{2}$$

Here, V_{ij} describes the coupling between radial and axial modes in the parameter space, which is due to the change of the resonator aspect ratio (the disk diameter for the fixed height). If $|C^a_{1,2}| \ll |C^b_{1,2}|$ or $|C^a_{1,2}| \gg |C^b_{1,2}|$, then the modes can be considered as dominantly radial or axial, otherwise, for $|C^a_{1,2}| \simeq |C^b_{1,2}|$ both modes are hybrid. The values V_{ij} can be extracted from the calculated dispersion $\omega_{1,2}$, by using the two-level model approximation.[19]

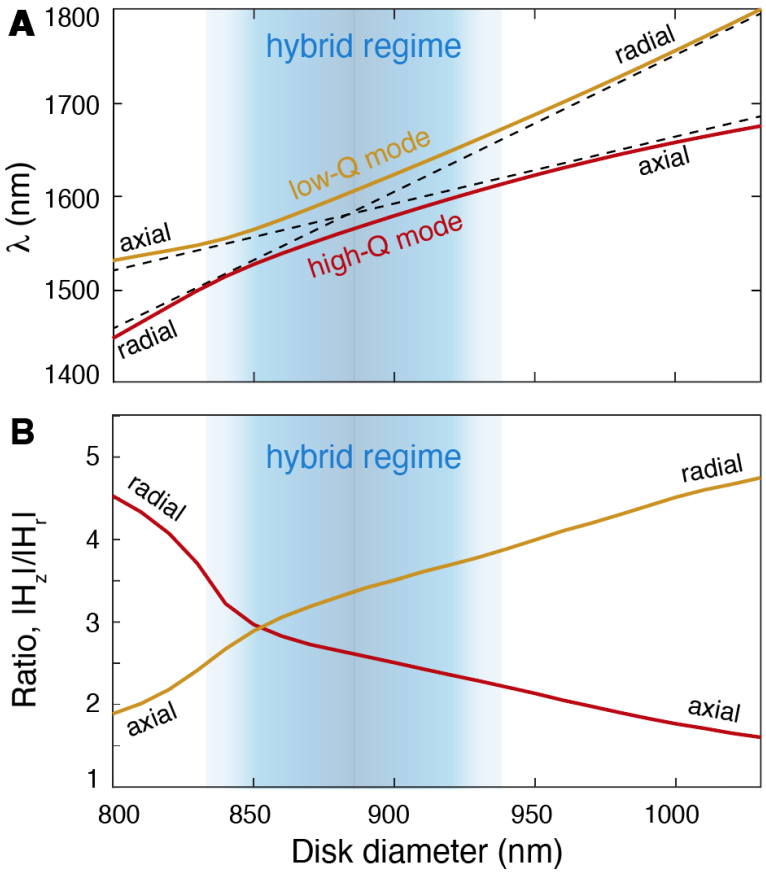

Figure 1. (A) Calculated mode wavelengths vs. resonator diameter for the disk on a structured substrate. The dashed lines qualitatively show the dispersion of uncoupled radial and axial modes. (B) Calculated ratio $|H_z|/|H_r|$ as a function of the disk diameter. The regime of hybrid modes is qualitatively shown by the blurred blue area.

To simplify the analysis of mode hybridization, it is also possible to compare the mode polarization ratio. For nanoresonator modes with fixed $m \neq 0$ and fixed p, the radial modes possess one dominant polarization (TE or TM), while the axial modes always have another polarization. Then, the criterion of mode hybridization is the degree of TE or TM polarization. For nanoresonator modes with fixed $m = 0$, such as the modes studied in the main text, the polarization is pure. For pure TE modes, as in the paper, which have only three nonzero field components E_φ, H_z, H_r in the cylindrical coordinate frame, the criterion of mode hybridization is the ratio of two nonzero magnetic field components, e.g. $|H_z|/|H_r|$, as shown in Fig. 1B. At the same time, the absolute value of the electric field component $|E_\varphi|$ is almost constant in the vicinity of the ARC. We also note that in the presence of the substrate, p is not a mode index any more and can be used only approximately, while the modes with different p can be hybridized in the vicinity of ARCs.

For numerical simulations of the linear spectrum, we use the finite-element-method solver in COMSOL Multiphysics in the frequency domain. To compare the simulations with the measured spectra, we consider the azimuthally polarized pump. To obtain the exact expression for the background field for scattering simulations, we derive the angular spectrum representation for the azimuthal cylindrical vector beam in each layer of the multilayered structure and match the solutions at the boundaries between the layers. We perform the multipolar decomposition of the total scattered power in the full solid angle shown in Fig. 2. It demonstrates that the quasi-BIC is manifested as a resonant feature and is determined by the magnetic dipolar and octupolar patterns.

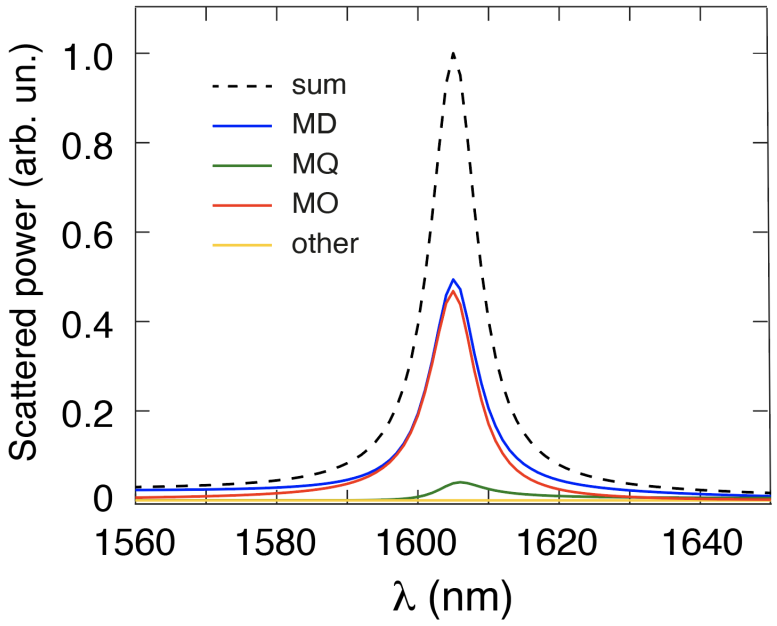

Figure 2. Multipolar decomposition of the scattered power at the pump wavelength in the full solid angle for a 930 nm disk on a three-layer substrate excited with an azimuthally polarized cylindrical vector pump.

3. ANALYSIS OF NONLINEAR RESPONSE.

We consider a subwavelength AlGaAs disk on a substrate. We neglect the absorption losses, since the material Q factor $\mathrm{Re}[\varepsilon]/\mathrm{Im}[\varepsilon] > 10^3$ within the range of wavelengths from 780 to 1670 nm. Also we neglect the losses due to surface roughness are low because of high quality of fabrication. The disk is excited by the pump with a given distribution of electric field $\mathbf{E}_{\mathrm{bg}}$. The total electric field $\mathbf{E}(\mathbf{r})$ in each point of the space can be divided into the background and the scattered as

$$\mathbf{E}(\omega, \mathbf{r}) = \mathbf{E}_{\mathrm{sc}}(\omega, \mathbf{r}) + \mathbf{E}_{\mathrm{bg}}(\omega, \mathbf{r}). \tag{3}$$

The scattered field can be found using the Green's function

$$\mathbf{E}_{\mathrm{sc}}(\omega, \mathbf{r}) = -\frac{\omega^2}{c^2} \int d\mathbf{r}' \ \Delta\epsilon(\omega, \mathbf{r}')\hat{\mathbf{G}}(\omega, \mathbf{r}, \mathbf{r}') \cdot \mathbf{E}_{\mathrm{bg}}(\omega, \mathbf{r}'), \tag{4}$$

where $\Delta\epsilon(\omega, \mathbf{r}) = \epsilon(\omega, \mathbf{r}) - \epsilon_{\mathrm{bg}}(\omega, \mathbf{r})$.

The scattered field can be rigorously expanded into a series of the resonator's eigenmodes. We consider the case when only one mode $\mathbf{E}_1$ is resonantly excited in the vicinity of the pump frequency

$$\mathbf{E}_{\mathrm{sc}}(\omega, \mathbf{r}) = a(\omega)\mathbf{E}_1(\mathbf{r}). \tag{5}$$

Next, we find the resonant amplitude a at the pump wavelength

$$a(\omega) = -\frac{\omega}{2N_1(\omega - \omega_1 + i\gamma_1)} \int d\mathbf{r}' \ \Delta\epsilon(\omega, \mathbf{r}')\mathbf{E}_1(\mathbf{r}') \cdot \mathbf{E}_{\mathrm{bg}}(\omega, \mathbf{r}'). \tag{6}$$

The energy accumulated inside the resonator $W(\omega)$ is proportional to $|a|^2$, which can be re-written as

$$W(\omega) \propto |a(\omega)|^2 = \frac{c}{N_1\omega_1} Q_1 L_1(\omega)\kappa_1(\omega)P_0'(\omega). \tag{7}$$

Here, $Q_j = \omega_j/2\gamma_j$ is the mode quality factor, the spectral overlap factor $L_j(\omega)$ is

$$L_j(\omega) = \frac{\gamma_j^2}{(\omega-\omega_j)^2+\gamma_j^2}, \tag{8}$$

and the coupling coefficient κ_1 is

$$\kappa_1(\omega) = \frac{\left|(\omega/c)\int d\mathbf{r}^{'}\ \Delta\epsilon(\omega,\mathbf{r}^{'})\mathbf{E}_1(\mathbf{r}^{'})\cdot\mathbf{E}_{\mathrm{bg}}(\omega,\mathbf{r}^{'})\right|^2}{(2\gamma_1/c)N_1P^{'}(\omega)}. \tag{9}$$

The coefficient $P^{'}(\omega)$ is proportional to the total incident power $P(\omega)$

$$P^{'}(\omega) = \frac{8\pi}{c}P(\omega). \tag{10}$$

To analyse the resonator response at the SH wavelength we calculate the nonlinear SH polarization $\mathbf{P}^{\mathrm{NL}}$

$$P_i^{\mathrm{NL}}(2\omega) = \sum_{j,k}\chi_{ijk}^{(2)}E_j(\omega)E_k(\omega), \tag{11}$$

where $\chi_{ijk}^{(2)}$ is the second-order susceptibility tensor. For AlGaAs $\chi^{(2)}$ has the symmetry of the zincblende crystalline structure. We assume the resonant conditions when the amplitude $a(\omega)$ is large, so $\mathbf{E}(\omega,\mathbf{r}) \simeq \mathbf{E}_{\mathrm{sc}}(\omega,\mathbf{r})$ and

$$P_i^{\mathrm{NL}}(2\omega) = [a(\omega)]^2\sum_{j,k}\chi_{ijk}^{(2)}E_{1,j}E_{1,k}. \tag{12}$$

The induced field $\mathbf{E}(2\omega)$ at the SH wavelength can be found using the resonator Green's function similar to Eq. (4)

$$\mathbf{E}(2\omega,\mathbf{r}) = -\frac{(2\omega)^2}{c^2}\int d\mathbf{r}^{'}\hat{\mathbf{G}}(2\omega,\mathbf{r},\mathbf{r}^{'})\cdot\mathbf{P}^{\mathrm{NL}}(2\omega,\mathbf{r}^{'}). \tag{13}$$

We assume that $\mathbf{E}(2\omega)$ is dominated by a single resonant state $\mathbf{E}_2$ with frequency ω_2 lying in the vicinity of 2ω

$$\mathbf{E}(2\omega,\mathbf{r}) = b(2\omega)\mathbf{E}_2(\mathbf{r}). \tag{14}$$

Thus, the amplitude b can be found as

$$b(2\omega) = -\frac{2\omega}{2N_2(2\omega-\omega_2+i\gamma_2)}\int d\mathbf{r}\ \mathbf{E}_2(\mathbf{r})\cdot\mathbf{P}^{\mathrm{NL}}(2\omega,\mathbf{r}) = \\ = -\frac{2\omega\,[a(\omega)]^2}{2N_2(2\omega-\omega_2+i\gamma_2)}\sum_{i,j,k}\chi_{ijk}^{(2)}\int d\mathbf{r}\ E_{2,i}E_{1,j}E_{1,k}. \tag{15}$$

The energy of the SH field is proportional to $|b(2\omega)|^2$

$$|b(2\omega)|^2 = \frac{(2\omega/c)^2}{(2\gamma_2/c)N_2}Q_2L_2(2\omega)\kappa_{12}\left[\frac{\omega_1}{c}N_1|a(\omega)|^2\right]^2, \tag{16}$$

where the cross-coupling coefficient κ_{12} is

$$\kappa_{12} = \frac{\left|\sum_{i,j,k}\chi_{ijk}^{(2)}\int d\mathbf{r}\ E_{2,i}(\mathbf{r})E_{1,j}(\mathbf{r})E_{1,k}(\mathbf{r})\right|^2}{(N_2\omega_2/c)(N_1\omega_1/c)^2}. \tag{17}$$

The total SH power

$$P(2\omega) = \frac{c}{8\pi}\oint_S d\mathbf{S}\cdot\mathrm{Re}\left[\mathbf{E}(2\omega)\times\mathbf{H}^*(2\omega)\right]. \tag{18}$$

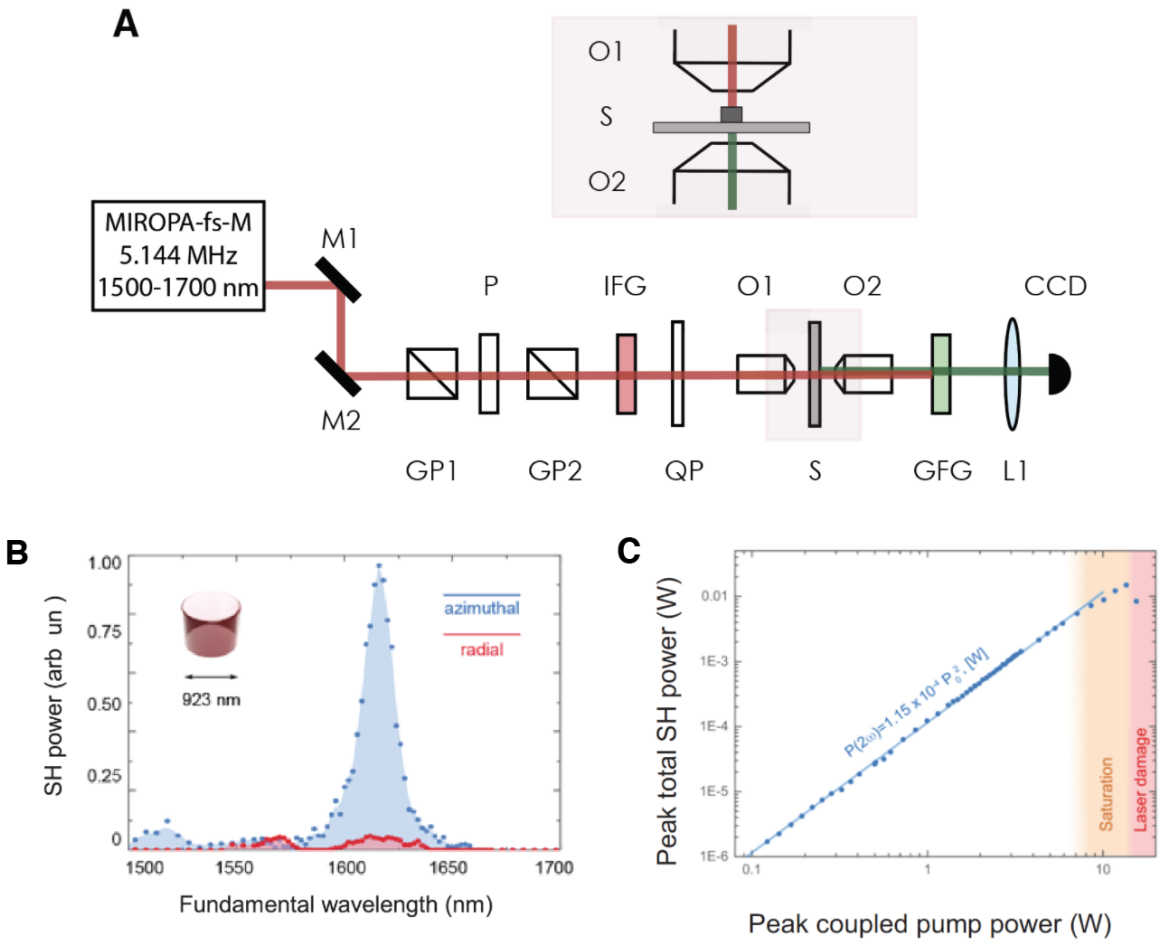

Figure 3. (A) Second-harmonic generation experimental setup in transmission. MIROPA-fs-M is the optical parametric amplifier, M1 and M2 are the mirrors, GP1 and GP2 are the Glan prisms, P is the wire-grid polarizer, IFG is the infrared glass filter, QP is the commercial liquid crystal q-plate, O1 and O2 are the objectives, S is the sample on a three-dimensional stage, GFG is the set of filters which transmit the SH signal, L1 is the lens, CCD is the detecting visible camera, DM is the dichroic mirror. (B) SH intensity spectrum for a disk with the diameter of 923 nm; (C) dependence of the total SH peak power on the peak pump power.

Here, the integral is evaluated at the disk surface, where Eq. (14) is valid.

Finally, we get the expression for the total SH power

$$P(2\omega) = \alpha(2\omega)\kappa_2 Q_2 L_2(2\omega)\kappa_{12}\left[Q_1 L_1(\omega)\kappa_1(\omega)P(\omega)\right]^2. \tag{19}$$

Here, the decoupling coefficient κ_2 is

$$\kappa_2 = \frac{\oint_S d\mathbf{S}\cdot \mathrm{Re}\left[\mathbf{E}_2 \times \mathbf{H}_2^*\right]}{(2\gamma_2/c)N_2}, \tag{20}$$

and the smooth envelope coefficient α is

$$\alpha(2\omega) = \frac{8\pi}{c}\left[\frac{2\omega}{c}\right]^2. \tag{21}$$

4. EXPERIMENTAL RESULTS

For experimental observation, we used AlGaAs nanodisks on a glass substrate. A set of nanoparticles with diffrent diameters are fabricated from a wafer consisted of a GaAs substrate, a sacrificial layer of AlInP and a 650-nm [100]-grown AlGaAs layer; then the pillars are transferred to a glass substrate. We generate a SHG signal in individual nanodisks by a tunable pulsed laser pump (pulse duration 300 fs, repetition rate 21 MHz). We generate two orthogonal states of cylindrical vector beams using an achromatic half-wave plate and a silicon-based spectrally broadband metasurface. The SHG signal from a single resonator is collected in forward direction by a visible objective (x100 0.9NA) and detected by a cooled CCD camera; then it is normalized over a spectral function of the experimental setup. The origin of a nonlinear signal is checked by its spectrum and corresponding power dependence. Figure 3 summarizes our experimental findings on SHG spectroscopy in individual AlGaAs nanocylinders.

5. CONCLUSIONS

We have analyzed the origin of high-Q resonances associated with bound states in the continuum in individual subwavelength nanoresonators. We have performed theoretical analysis of SHG in such nanoresonators in the regime of BICs. In experiment, we have employed a structured pump beam to generate the second-harmonic from isolated AlGaAs nanoparticles, and conduct nonlinear spectroscopic measurements. We have demonstrated experimentally optical resonances governed by bound states in the continuum in individual AlGaAs nanoparticles with the record-high SHG efficiency being empowered by the enhanced field confinement associated with high-Q resonant modes.

ACKNOWLEDGMENTS

The authors acknowledge a financial support from the Australian Research Council (ARC), the Russian Foundation for Basic Research (18-32-20205), and the National Research Foundation of Korea (NRF) under grant no. 2018R1A3A3000666 funded by the Korean Government (MSIT). K.K. and A.B. acknowledge support from the Foundation for the Advancement of Theoretical Physics and Mathematics "BASIS".

REFERENCES

[1] Kuznetsov, A. I., Miroshnichenko, A. E., Brongersma, M. L., Kivshar, Y. S., and Luk'yanchuk, B., "Optically resonant dielectric nanostructures," *Science* **354**(6314), aag2472 (2016).

[2] Staude, I. and Schilling, J., "Metamaterial-inspired silicon nanophotonics," *Nature Photonics* **11**(5), 274 (2017).

[3] Lin, D., Fan, P., Hasman, E., and Brongersma, M. L., "Dielectric gradient metasurface optical elements," *Science* **345**(6194), 298–302 (2014).

[4] Arbabi, A., Horie, Y., Bagheri, M., and Faraon, A., "Dielectric metasurfaces for complete control of phase and polarization with subwavelength spatial resolution and high transmission," *Nature Nanotechnology* **10**(11), 937 (2015).

[5] Kruk, S. and Kivshar, Y., "Functional meta-optics and nanophotonics governed by mie resonances," *ACS Photonics* **4**(11), 2638–2649 (2017).

[6] Kivshar, Y., "All-dielectric meta-optics and non-linear nanophotonics," *National Science Review* **5**(2), 144–158 (2018).

[7] von Neumann, J. and Wigner, E. P., "Über merkwürdige diskrete eigenwerte," in [*The Collected Works of Eugene Paul Wigner*], 291–293, Springer (1993).

[8] Marinica, D., Borisov, A., and Shabanov, S., "Bound states in the continuum in photonics," *Physical Review Letters* **100**(18), 183902 (2008).

[9] Hsu, C. W., Zhen, B., Lee, J., Chua, S.-L., Johnson, S. G., Joannopoulos, J. D., and Soljačić, M., "Observation of trapped light within the radiation continuum," *Nature* **499**(7457), 188 (2013).

[10] Hsu, C. W., Zhen, B., Stone, A. D., Joannopoulos, J. D., and Soljačić, M., "Bound states in the continuum," *Nature Reviews Materials* **1**(9), 16048 (2016).

[11] Koshelev, K., Favraud, G., Bogdanov, A., Kivshar, Y., and Fratalocchi, A., "Nonradiating photonics with resonant dielectric nanostructures," *Nanophotonics* **8**(5), 725–745 (2019).

[12] Koshelev, K., Bogdanov, A., and Kivshar, Y., "Engineering with bound states in the continuum," *Optics and Photonics News* **31**(1), 38–45 (2020).

[13] Kodigala, A., Lepetit, T., Gu, Q., Bahari, B., Fainman, Y., and Kanté, B., "Lasing action from photonic bound states in continuum," *Nature* **541**(7636), 196 (2017).

[14] Koshelev, K. and Kivshar, Y., "Light trapping gets a boost," *Nature* **574**, 491 (2019).

[15] Koshelev, K., Bogdanov, A., and Kivshar, Y., "Meta-optics and bound states in the continuum," *Science Bulletin* **64**(12), 836–842 (2019).

[16] Rybin, M. V., Koshelev, K. L., Sadrieva, Z. F., Samusev, K. B., Bogdanov, A. A., Limonov, M. F., and Kivshar, Y. S., "High-Q supercavity modes in subwavelength dielectric resonators," *Physical Review Letters* **119**(24), 243901 (2017).

[17] Sadrieva, Z. F., Sinev, I. S., Koshelev, K. L., Samusev, A., Iorsh, I. V., Takayama, O., Malureanu, R., Bogdanov, A. A., and Lavrinenko, A. V., "Transition from optical bound states in the continuum to leaky resonances: role of substrate and roughness," *ACS Photonics* **4**(4), 723–727 (2017).

[18] Carletti, L., Koshelev, K., De Angelis, C., and Kivshar, Y., "Giant nonlinear response at the nanoscale driven by bound states in the continuum," *Physical Review Letters* **121**(3), 033903 (2018).

[19] Bogdanov, A. A., Koshelev, K. L., Kapitanova, P. V., Rybin, M. V., Gladyshev, S. A., Sadrieva, Z. F., Samusev, K. B., Kivshar, Y. S., and Limonov, M. F., "Bound states in the continuum and fano resonances in the strong mode coupling regime," *Advanced Photonics* **1**(1), 016001 (2019).